

Constraints on dark matter models from the observation of Triangulum-II with the *Fermi* Large Area Telescope

Sayan Biswas^{1,*}, Pooja Bhattacharjee^{2,3,†}, Pratik Majumdar^{4,‡},
Subinoy Das^{5,§}, Mousumi Das^{5,¶} and Partha S. Joarder^{2,3,**}

¹ Raman Research Institute, C.V. Raman Avenue,
Sadashivanagar, Bangalore, Karnataka 560080, India

² Department of Physics, Bose Institute, 93/1 A.P.C. Road, Kolkata 700009, India

³ Centre for Astroparticle Physics and Space Science, Bose Institute,
Block EN, Sector V, Salt Lake, Kolkata 700091, India

⁴ Saha Institute of Nuclear Physics, HBNI, 1/AF, Bidhannagar, Kolkata 700064, India and

⁵ Indian Institute of Astrophysics, Koramangala, Bangalore, Karnataka 560034, India

Triangulum-II, a newly discovered dwarf spheroidal galaxy, is a strong candidate for the indirect search of dark matter through the detection of γ -ray emission that could originate from the pair-annihilation of weakly interacting massive particles (WIMPs). We here report on the analysis of almost seven years *Fermi* Gamma-Ray Space Telescope data of Triangulum-II which was taken during its all sky survey operation mode. No excess γ -ray emission has been detected above 100 MeV from Triangulum-II. We derive the upper limits on γ -ray flux assuming both the power-law spectra and the spectra related to WIMP annihilation. In this work, we have considered several theoretical WIMP (neutralinos here) models envisioning both thermal and non-thermal production of WIMPs, and put limits on pair-annihilation cross-section of WIMPs to constrain the parameter space related to those theoretical models.

Keywords: dark matter, WIMP, dwarf spheroidal galaxy.

1. INTRODUCTION

Recent high precision data on cosmic microwave background (CMB) [1, 2] indicates that some form of non-luminous and non-baryonic matter, usually known as dark matter (DM), constitutes around 75% mass density of the total mass density in the Universe. However, very little is known about the underlying nature of DM even after the strenuous efforts of several high energy physicists, astrophysicists and cosmologists over many years. It still remains as one of the most fascinating and intriguing areas of research in modern physics. Cosmological simulations, experimental evidences and theoretical arguments in recent times mostly favour the existence of non-baryonic cold dark matter (CDM) candidates to explain the formation of observed large-scale structures in the Universe [3]. But the actual constituents of CDM are still unknown to us. A possible candidate is a new type of weakly interacting massive particles (WIMPs) that is considered to be the constituent of CDM [3–5]. On theoretical grounds, WIMPs, predicted to exist in several theories related to beyond the Standard Model of particle physics, are possibly the best motivated candidates for CDM as the inferred thermal abundance obtained from the typical pair-annihilation cross section of such WIMPs for their natural mass range (i.e. between few GeV to few TeV) is within the range comparable to the estimated values of cosmological DM calculations. Generally, it is believed that pair-annihilation (or decay) of WIMPs can also occur in the present epoch and will yield high-energy γ rays [3]. Hence, detection of such high-energy γ rays is a valuable tool that will indirectly provide us the information about the nature of DM. In this paper, we assume that WIMPs are stable and consider only the pair-annihilation of such WIMPs to analyze the high-energy γ -ray data collected by the *Fermi* satellite [6]. According to cosmological N-body simulations for structure formation, the DM halos formed by WIMPs are not smooth rather they contain a large number of bound substructures (or subhalos) whose numbers increase with decreasing mass of WIMPs [3, 7–9]. These smaller halos (or subhalos) around the large galaxy halo can be observationally identified as dwarf spheroidal galaxies (dSphs). From the point of view of CDM scenario those dSphs would be considered as one of the densest DM regions, along with they are also believed to be

*sayan@rri.res.in

†pooja.bhattacharjee@jcbose.ac.in

‡pratik.majumdar@saha.ac.in

§subinoy@iiap.res.in

¶mousumi@iiap.res.in

**partha@jcbose.ac.in

the largest galactic substructures around our Milky Way Galaxy. Moreover, the mass-to-light ratio in dSphs is of the order 100 – 1000 which implies that they are largely DM dominated galaxies. Apart from that, dSphs do not show γ -ray emission from other astrophysical sources such as star forming regions, active galactic nuclei (AGN) and there is no observational evidence indicating the presence of neutral or ionized gas in these galaxies [10]. Hence, such dSphs are the ideal sites for indirect DM search.

In recent past, Sloan Digital Sky Survey (SDSS) [11] discovered a new population of Milky Way satellites which are ultra-faint and possibly DM dominated dSphs [12–17]. Indeed, over the past year or so, Panoramic Survey Telescope and Rapid Response System (Pan-STARRS) [18] and the Dark Energy Survey (DES) [19] have found new candidate dSphs [20–23] in the vicinity of Milky Way. Triangulum-II (Tri-II), one of these new dSphs, has recently been found by Pan-STARRS Survey [20] and it appears to be an ultra-faint and DM dominated dwarf galaxy or globular cluster. Recent calculations [24, 25] also claim that it would be a very good target to search for pair-annihilation of WIMPs.

We have organized the paper in the following manner. In Section 2 we will briefly discuss about the properties of Tri-II and describe our analysis procedure of *Fermi* data of Tri-II and how we obtained the upper limit to γ -ray fluxes using the power-law spectra with different spectral indices. In the next section, we model the DM density of Tri-II with a suitable density profile and discuss the necessary parameters that are needed to obtain the γ -ray flux due to pair-annihilation of WIMPs (Section 3.1). In Section 3.2, we determine the upper limit to γ -ray fluxes using the spectra resulting from annihilation of various WIMP models with different WIMP masses. We will also determine the upper limit to pair-annihilation cross-sections and discuss the implication in the context of different WIMP models (Section 3.2). In Section 4, we will summarize our conclusions.

2. FERMI-LAT OBSERVATION AND DATA ANALYSIS OF TRIANGULUM-II (TRI-II)

2.1. Triangulum-II

TABLE I: Some properties of Tri-II

Property	Value	Reference
Galactic latitude	141.4°	[20]
Galactic longitude	−23.4°	[20]
Galactocentric distance	36 $^{+2}_{-2}$ kpc	[24, 27]
2D half light radius (r_h)	34 $^{+9}_{-8}$ pc	[27, 28]
Velocity relative to Galactic standard of rest (GSR) (v_{GSR})	−261.7 km s $^{-1}$	[28]
Mean heliocentric velocity $\langle v_{\text{helio}} \rangle$	−381.7 ± 1.1 km s $^{-1}$	[28]
Stellar Velocity Dispersion (σ_v)	< 3.4 km s $^{-1}$ (90% C.L.)	[28]
	< 4.2 km s $^{-1}$ (95% C.L.)	[28]
Mass within 3D half-light radius ($\frac{M_{1/2}}{M_{\odot}}$)	< 3.7 × 10 5 (90% C.L.)	[28]
	< 5.6 × 10 5 (95% C.L.)	[28]
Mass-to-light ratio within 3D half-light radius ($(M/L_v)_{1/2}$)	< 1640 M $_{\odot}$ L $_{\odot}^{-1}$ (90% C.L.)	[28]
	< 2510 M $_{\odot}$ L $_{\odot}^{-1}$ (95% C.L.)	[28]
Density within 3D half-light radius $\rho_{1/2}$	< 2.2 M $_{\odot}$ pc $^{-3}$ (90% C.L.)	[28]
	< 3.3 M $_{\odot}$ pc $^{-3}$ (95% C.L.)	[28]
Metallicity ([Fe/H])	−2.24 ± 0.05	[28]

Note: M_{\odot} and L_{\odot} denote the mass and luminosity of the Sun respectively.

According to our current knowledge, Tri-II appears to be a metal-poor dwarf galaxy with few stars in it and having a large mass-to-light ratio [27, 28]. The exact number of stars in Tri-II is yet to be confirmed. In the previous studies, one group of observers studied 13 member stars [26] while another group studied 6 member stars [27] in Tri-II. Recently, Kirby and his collaborators updated their previous estimates by studying 13 member stars in Tri-II [28]. The revised values of the velocity dispersion of the stars in Tri-II are $< 4.2 \text{ km s}^{-1}$ for 95% C.L. and $< 3.4 \text{ km s}^{-1}$ for 90% C.L. [28] respectively. We have tabulated some properties of Tri-II in Table 1.

The quantities such as $M_{1/2}$, $(M/L_v)_{1/2}$ and $\rho_{1/2}$ have been calculated by presuming that Tri-II is spherically symmetric and it is in dynamical equilibrium. Although, it is still not clear whether Tri-II is in dynamical equilibrium or it has been disrupted by tidal force. Various properties such as large velocity (relative to GSR) and low ellipticity indicate that Tri-II would not be affected much by the total tidal effect [27] which may give hint about the dynamical equilibrium. On the other hand, Tri-II is considered to be possibly associated with Triangulum-Andromeda halo substructures [20, 29] or the PAndAS stream [30], but the measurements by Deasen et al. [31] showed that the GSR velocities of such halo debris (i.e. halo substructures of Triangulum-Andromeda halo or the PAndAS stream) are quite different from the v_{GSR} of Tri-II which implies that Tri-II could not be associated with any (presently) known stream [27]. This, in fact, does not prove the dynamical equilibrium of Tri II, rather, it implies, if Tri-II is being tidally disrupted, it is not the source of stellar debris of Triangulum-Andromeda or PAndAS [27]. Hence, the issue related to the dynamical equilibrium of Tri-II is yet to be resolved. However, in this paper we have considered that Tri-II is in dynamical equilibrium.

2.2. *Fermi* data analysis of Triangulum-II

The *Fermi*-LAT is a space based γ -ray detector, launched on June 11, 2008 by a Delta II Heavy launch vehicle [6], that can detect γ rays in the energy range of 20 MeV to 300 GeV [32]. In our analysis for Tri-II, we have used the data taken by *Fermi*-LAT during almost its 7 years of sky survey operation (i.e. from August 4, 2008 to May 22, 2015).

In our analysis, we use `Fermi ScienceTools` version v10r0p5, a software package which is dedicated for the analysis of *Fermi*-LAT data [33]. For the data analysis, we have chosen a region of interest (ROI) such that it covers a 10° region around Tri-II. We also apply a cut on reconstructed energy E so that E is in the range of 100 MeV to 50 GeV. The range is chosen to achieve a good signal response. Next, we have analyzed our dataset using binned likelihood technique as implemented in the `ScienceTools` [34, 35]. We have used event class 128 and event type 3 along with we have also used the version of P8R2_SOURCE_V6 of instrument response function (IRF) [36] for our analysis. In the desired ROI, the source model includes all the sources of *Fermi* 4-year catalogue which are within the 10° radius of Tri-II. The sources are modelled as point-like with power-law which is considered to be a reasonable approximation in the absence of any rigorous studies of them. During the fitting procedure, the position and spectral parameters of these sources are kept free. Moreover, the models, currently used by the LAT-collaboration, of Galactic diffusion emission and the isotropic component (which includes any extragalactic diffusion emission and any residual charged background contamination) are also used by us in this analysis. To take into account the uncertainties in modelling those diffuse components, the independent normalizations of such diffuse components are kept free during the fit. Finally, Tri-II is modelled as a point-source by keeping fixed its localization during the fitting procedure. This assumption is reasonable in the context of angular resolution of the LAT. In this paper, we have modelled the source spectra by following two strategies: first we apply model-independent power-law spectra for various spectral indices which is discussed in Sec. 2.3 and then we employ γ -ray spectra which represent the possible pair-annihilation of WIMPs for wide ranges of masses and for several WIMP models (see Sec. 3.2).

2.3. Results from power-law modelling

The differential flux can be written as a power-law spectrum (i.e. number of photons within the area interval dA , energy interval dE and time interval dt) can be written as [3]

$$\frac{dN}{dAdEdt} = N_0 \left(\frac{E}{E_0} \right)^{-\Gamma}, \quad (1)$$

where, N_0 is the normalization parameter, Γ is the power-law index, E is the reconstructed energy of photon with E_0 is an arbitrary energy scale which is set at 100 MeV. In this paper, we have restricted E in the range 100 MeV to 50 GeV. In Eq. (1), N_0 and Γ are two unknown parameters which have to be determined by fitting the astrophysical source spectrum. In our analysis, we have fixed Γ to five possible values; $\Gamma = 1, 1.8, 2, 2.2, 2.4$. Among those power-law indices, the first index, i.e. $\Gamma = 1$, is chosen by the DM annihilation models in Ref. [37] whereas, other four indices are

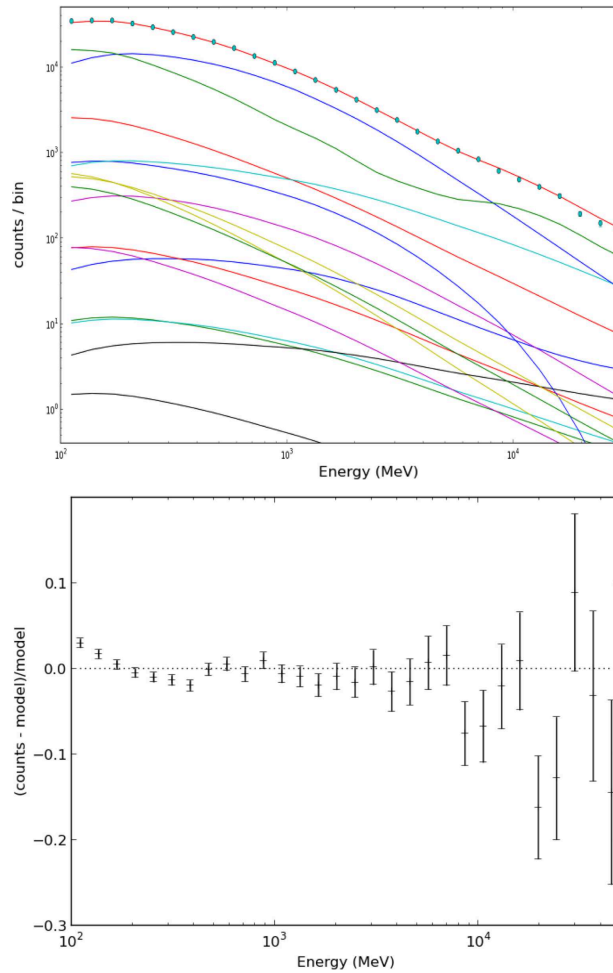


FIG. 1: Spectral fit to the counts (top panel) and the corresponding residual plot (bottom panel) for the ROI around Tri-II have been shown in the figures. The top red line (top panel) shows the summed model and the corresponding data points in the best fit total spectrum for index $\Gamma = 2$ with power-law model around the ROI. The top blue and green lines (top panel) show the Galactic diffuse component and isotropic component respectively and the rest coloured lines in the spectral plot (top panel) are for other point sources in the chosen ROI.

used to determine the constraint on standard astrophysical source spectrum. We have repeated the binned likelihood analysis for each index and for the chosen ROI. In each analysis, N_0 is then fitted to the data along with the isotropic and Galactic diffuse normalizations.

In Table 2, we have shown the best-fit values of the normalization (i.e. N_0) with the corresponding errors and test statistics (TS) values (i.e. proportional to the logarithm of the ratio of the maximum likelihood value for a model without source to the maximum likelihood value for a model with the desired source at a specific position) for five different indices. Second column of Table 2 shows that the errors are higher than the values of N_0 itself. The above findings imply that no significant signal from the direction of Tri-II has been detected. Figs. 1(a,b) show the spectral fit to data and residual of that fit for Tri- II with $\Gamma = 2$.

As no significant signal has been detected in the direction of Tri-II, we have then derived the flux upper limit. The flux upper limit has been evaluated over the full dataset (i.e. in the range 100 MeV to 50 GeV) using profile likelihood method [38, 39]. In profile likelihood method, N_0 of Tri-II has been calculated with 95% confidence level (C.L.) with the other two free parameters, i.e. the normalizations of the two diffuse backgrounds, are fitted at each step. This scanning procedure continues until the difference of the logarithm of likelihood function reaches the value 1.35 [3] corresponding to a one-sided 95% confidence level (C.L.). We then applied the Bayesian method, as implemented in the `Fermi ScienceTools` [3], to obtain a more appropriate value of the upper limit with 95% C.L. In Table 3, we have tabulated the γ -ray flux upper limits in the whole energy range (i.e. 100 MeV to 50 GeV) for different spectral indices. It is seen from Table 3. that the flux upper limit for $\Gamma = 1$ is about 16 times lower than the flux upper limit of $\Gamma = 2.4$.

TABLE II: Fitted values of the normalization parameter and TS values for five different spectral indices (Γ) in the chosen ROI.

Spectral Index (Γ)	$N_0 \times 10^{-5}$	Test Statistic (TS) value
1	$(1.41 \pm 2.75) \times 10^{-9}$	0.41
1.8	$(6.66 \pm 11.49) \times 10^{-8}$	0.44
2	$(1.06 \pm 2.41) \times 10^{-7}$	0.23
2.2	$(1.88 \pm 5.53) \times 10^{-7}$	0.02
2.4	$(1.41 \pm 2.75) \times 10^{-11}$	-7.45×10^{-8}

TABLE III: Flux upper limits of Triangulum-II at 95% C.L.

Spectral Index (Γ)	Flux upper limits at 95% C.L. ($\text{cm}^{-2} \text{sec}^{-1}$)
1	8.29×10^{-11}
1.8	4.55×10^{-10}
2	7.14×10^{-10}
2.2	1.04×10^{-9}
2.4	1.37×10^{-9}

3. A THEORETICAL FRAMEWORK TO ESTIMATE γ -RAY FLUX FROM PAIR-ANNIHILATION OF WIMPS IN CASE OF TRIANGULUM-II

3.1. Modelling of the dark matter density profile of Triangulum-II

In Tri-II, at a photon energy E , the γ -ray flux within a solid angle $\Delta\Omega$ which is originated from pair-annihilation of WIMPs, each having a mass m_{WIMP} , is given by [3, 25, 40]

$$\phi_{\text{WIMP}}(E, \Delta\Omega) = \Phi^{pp}(E) \times J(\Delta\Omega), \quad (2)$$

where, $\Phi^{pp}(E)$ and $J(\Delta\Omega)$ can be denoted as ‘‘particle physics factor’’ and ‘‘astrophysical factor’’ (or ‘‘J factor’’) respectively.

3.1.1. Particle Physics factor

$\Phi^{pp}(E)$ depends only on the characteristic of the candidate particle such as WIMP in our case and it can be defined as [3]

$$\Phi^{pp}(E) = \frac{\langle \sigma v \rangle}{8\pi m_{\text{WIMP}}^2} \sum_f \frac{dN_f}{dE} B_f. \quad (3)$$

In Eq. (3), $\langle \sigma v \rangle$ is the product of relative velocity and the annihilation cross-section of two WIMPs which is (thermally) averaged over their velocity distributions [3]. Here, f indicates the possible pair-annihilation final states with $\frac{dN_f}{dE}$ and B_f being the γ -ray spectrum (i.e. number of photons per energy) and branching fraction corresponding to a f^{th} final state respectively. We would like to add that, here, we did not consider the Sommerfeld enhancement [3, 41, 42] i.e. the increment in γ -ray flux due to dependence of annihilation cross-section on relative velocity of particles. This factor comes in as the relative velocity of thermal relics at freeze-out is different than at the present epoch. Hence, the numerical value of annihilation cross-section may differ. Sommerfeld enhancement factor takes into account that mismatch in relative velocity and maximizes the signal by a factor 7 to 90 for DM mass in the range of 100 GeV to 3 TeV [42]. In order to be conservative, we did not include such effect.

3.1.2. Astrophysical factor

Astrophysical factor or J-factor is related to DM density distribution in the Tri-II. The J-factor can be defined as

$$\begin{aligned}
 J(\Delta\Omega) &= \int \int \rho^2(r(\lambda)) d\lambda d\Omega \\
 &= 2\pi \int_{\theta_{\min}}^{\theta_{\max}} \sin\theta \int_{\lambda_{\min}}^{\lambda_{\max}} \rho^2(r(\lambda)) d\lambda d\theta.
 \end{aligned}
 \tag{4}$$

Here, $\rho(r)$ is the assumed mass density of DM in Tri-II with r being the distance from its center and λ is the line-of-sight distance and $r(\lambda)$ is the galactocentric distance which can be denoted as $r(\lambda) = \sqrt{\lambda^2 + d^2 - 2\lambda d \cos\theta}$ with d being the distance of the Tri-II from the Earth (i.e. the heliocentric distance) and θ is the angle between the direction of observation and the center of Tri-II.

In this paper, we have modelled the mass density of the DM distribution of Tri-II with Navarro-Frenk-White (NFW) density profile [43]. For NFW density profile, we can use the following relation to calculate J-factor [44], i.e.

$$J \approx \frac{25}{8G^2} \frac{\sigma_v^4 \theta}{dr_h^2}.
 \tag{5}$$

where, σ_v is the velocity dispersion, r_h is 2D projected half light radius and G is the gravitational constant. We have observed that the estimated values of J-factor from the above relation are in good agreement with the numerically estimated values of J-factor for different dSphs. For our calculation purpose, we have considered $\theta = 0.13^\circ$. In Table 4., we have shown two different J-values corresponding to two different σ_v .

TABLE IV: Different parameters to calculate the astrophysical factor (J), see text for details.

d (kpc) [20]	σ_v (km sec ⁻¹) [28]	r_h (pc) [28]	θ (deg)	J-factor from Eq. 5 (GeV ² cm ⁻⁵)
30 ± 2	4.2 (95% C.L.)	34	0.13°	0.15 × 10 ²⁰
30 ± 2	3.4 (90% C.L.)	34	0.13°	0.64 × 10 ¹⁹

In our J-factor calculation, we did not take into account the contribution due to the annihilation in cold and dense substructures in Tri-II which in principle can increase the value of J [3]. However, we did not include such effect for the present calculation as the previous studies have shown that such effect can boost the J-factor by only a factor of few [3, 46].

3.2. Constraints on annihilation cross-section

Using Eq. (2), the estimated J-value from Eq. (4) (see. Table 4) and DMFit package [47], as implemented in the `ScienceTools`, 95% C.L. upper limits on γ -ray fluxes (above 100 MeV) and on $\langle \sigma v \rangle$ have been obtained as a function of the WIMP mass for specific annihilation channels. For our analysis, we have chosen pair-annihilation final states such as $b\bar{b}$, $\tau^+\tau^-$, $\mu^+\mu^-$ and W^+W^- . Such final states, in particular, are highly motivated by the case of neutralino candidates predicted by supersymmetry [5]. Previously, such annihilation final states have been also used to study the *Fermi* data of dSphs [3]. Although, our choice of final states is motivated here by the supersymmetry, the results presented in this section are not restricted only for neutralinos rather they are applicable for generic WIMP models.

In Fig. 2, we have shown the variation of the upper limits on the photon fluxes corresponding to various annihilation final states, such as 100% $b\bar{b}$, 100% $\tau^+\tau^-$, 80% $b\bar{b}$ + 20% $\tau^+\tau^-$, 100% $\mu^+\mu^-$ and 100% W^+W^- (these percentages are also useful for the direct comparison of our results with the previous results of dSphs), with the mass of WIMP. Among those final annihilation states producing hard γ -ray spectrum, the results for $\mu^+\mu^-$ and $\tau^+\tau^-$ are considered to be the best upper limits as they predict abundant photon flux at higher energies where the diffuse background is lower. Fig. 2 also shows that for $m_{\text{DM}} \sim 1$ TeV the upper limits related to all final states vary within a factor of 3 whereas at lower masses that variation is more than one order of magnitude. The results, as shown in Fig. 2, do not depend on any particular particle theory since they are based only on the final states of WIMP annihilation. We consider now few specific models to study the annihilation cross-section of WIMPs.

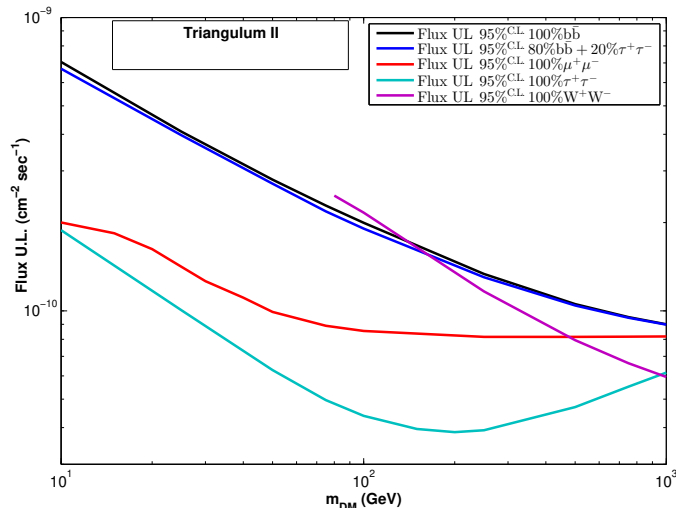


FIG. 2: Derived upper limits on γ -ray fluxes of Tri-II for various annihilation final states are shown in the figure.

In Figs. 3(a,b) and Fig. 4, we have compared the resulting LAT sensitivity for Tri-II for two velocity dispersion and also for a well known dSph, namely, Ursa Minor (UMi), the later being produced by us from the Fermi-LAT archival data for an observational period of 11 months, with different predictions from the different theoretical models. In this list first two models are minimal supergravity (mSUGRA) [48] and Minimal Supersymmetric Standard Model (MSSM) [49]. mSUGRA is a theoretically motivated DM model. In this model, the supersymmetry breaking parameters are specified at high energy scale which is typically of the order of grand unification scale $\sim 2 \times 10^{16}$ GeV. On the other hand, all the supersymmetry breaking parameters of MSSM are defined in the electro-weak energy (low energy) scale. Next, we have considered the anomaly mediated supersymmetry breaking (AMSB) model [50] where the supersymmetry breaking scenario may produce wino-like neutralinos or winos (i.e. a mass eigenstate of neutralino which corresponds to the supersymmetric fermionic partners of the SU(2) gauge bosons of the Standard Model). For about 2 TeV wino mass, the universal DM density matches with the thermal relic density produced by winos. Several non-thermal production scenarios also exist that could explain the wino DM scenario with lighter (i.e. DM mass is less than a TeV) DM candidates [3]. The last one is the lightest Kaluza-Klein particle of universal extra dimensions (UED) [51–53]. In this model, in the minimum setup, the first order excitation of the U(1) hypercharge gauge boson which is also commonly known as $B^{(1)}$ is related to the DM candidate. Actually in this case, an almost exact relationship exists between DM mass and its pair annihilation cross-section, and a thermal relic abundance related to DM density can be obtained for DM masses around 700 GeV [3, 52].

In Figs. 3(a,b) and Fig. 4, we have compared the LAT sensitivity, obtained during the analysis of *Fermi* data of Tri-II with DMFit package, in the $(m_{\text{DM}}, < \sigma v >)$ plane with the predicted estimates from our four selected DM models namely mSUGRA, MSSM, Kaluza-Klein DM in UED and wino-like DM in AMSB. Red points, in Figs. 3(a,b), are consistent with the 3σ WMAP constraint on the universal matter density in accord with thermal production while the blue points would indicate the lower thermal relic density [3]. In this paper, we assume that the blue points are related to non-thermal production mechanism of WIMPs in order to explain the observed universal matter density, and this kind of assumption was also taken in Ref. [3]. The advantage of such assumption is that neutralino density needs not to be rescaled which would be the case if we would assume exclusive thermal production scenario. Such non-thermal production scenario of WIMPs has been envisioned by various theories. For an example, several string-theory motivated frameworks predict that the generic decay of moduli produce Standard Model particles along with their supersymmetric partners, and those supersymmetric partners will eventually decay into the lightest neutralinos [54]. Apart from that, decay of topological objects such as Q-balls may produce neutralinos out of equilibrium [55]. A scenario that predicts the presence of a dynamical “quintessence” field in a kinematic-dominated phase [56, 57] also supports such non-thermal production of WIMPs.

Figs. 3(a,b) and 4 show the upper limits on $< \sigma v >$ for Tri-II for two different values of velocity dispersion, one an optimistic values of $\sigma_v < 4.2$ km sec^{-1} and another a rather conservative value of $\sigma_v < 3.4$ km sec^{-1} as determined by [28] along with the predictions from mSUGRA, MSSM, AMSB and Kaluza-Klein UED models respectively. In addition, we also compared our results with UMi, one of the best known candidates of DM. It is seen from Figs. 3(a,b) that even for a low velocity dispersion value of 3.4 km sec^{-1} , the constraints obtained on mSUGRA and MSSM

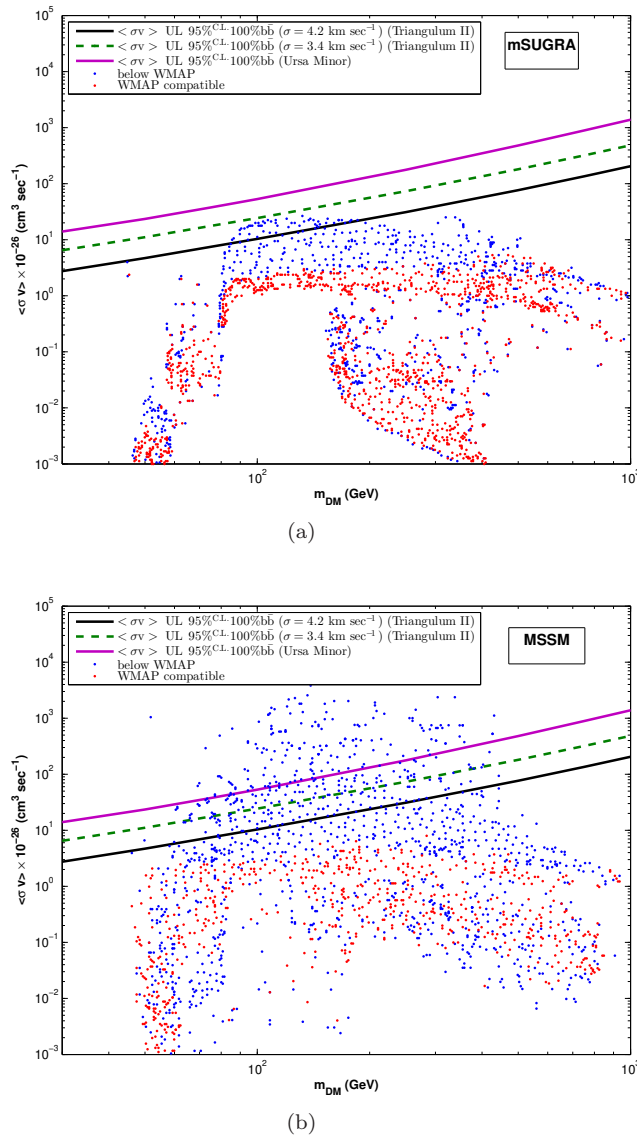


FIG. 3: Predictions from (a) mSUGRA and (b) MSSM models are plotted in $(m_{\text{WIMP}}, \langle\sigma v\rangle)$ plane. The red points (in the two panels) denote neutralino thermal relic abundance related to the inferred cosmological DM density and the blue points correspond to lower thermal relic density. The upper limit on $\langle\sigma v\rangle$ for two velocity dispersion value ([28]) of Tri-II with 95% C.L. for $\text{b}\bar{\text{b}}$ and the upper limit on $\langle\sigma v\rangle$ for UMi with 95% C.L. for $\text{b}\bar{\text{b}}$ are shown in the plots. The data of red and blue points are obtained from Ref. [3] and we have produced the data of UMi using the DMFit package and the parameter set used in Ref. [3].

models with low thermal densities are almost a factor 2.5 lower than that obtained from UMi for $m_{\text{WIMP}} = 100$ GeV. The constraints improve to a factor of ~ 6 if one considers a velocity dispersion of 4.2 km sec^{-1} . Furthermore, Fig 4 also indicates that for $\sigma_v = 4.2 \text{ km sec}^{-1}$ the upper limits on $\langle\sigma v\rangle$ disfavor the Kaluza-Klein in UED and AMSB models with masses $\lesssim 230$ GeV and $\lesssim 375$ GeV respectively. For $\sigma_v = 3.4 \text{ km sec}^{-1}$, the AMSB models are disfavored for masses $\lesssim 300$ GeV. However, no effective constraints can be put on Kaluza-Klein in UED models for such a conservative velocity dispersion. It must also be noted that we have only presented the results for 100% $\text{b}\bar{\text{b}}$ channel as it puts stronger constraints on the theoretical models than the other channels considered in the paper. We conclude that our results can put strong constraints on the models based on 200 GeV mass wino which is considered in Ref. [58]. We also point out that similar conclusions were also arrived at from the analysis of other dSphs [3].

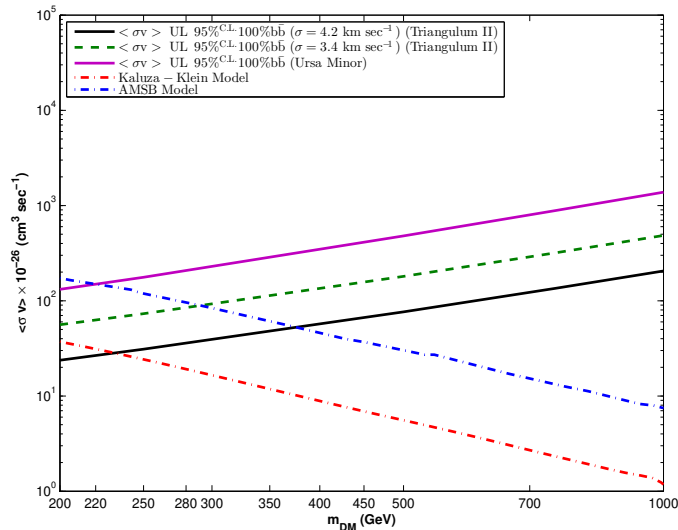


FIG. 4: Predictions from AMSB and Kaluza-Klein UED models are plotted in $(m_{\text{WIMP}}, \langle \sigma v \rangle)$ plane. The upper limit on $\langle \sigma v \rangle$ for two velocity dispersion value ([28]) of Tri-II with 95% C.L. for $b\bar{b}$ and the upper limit on $\langle \sigma v \rangle$ for UMi with 95% C.L. for $b\bar{b}$ are shown in the plots. The data of Kaluza-Klein UED and AMSB models are obtained from Ref. [3] and we have produced the data of UMi using the DMFit package and the parameter set used in Ref. [3].

4. CONCLUSIONS

In this work, we have analyzed the γ -ray data in the direction of Tri-II by `Fermi ScienceTools`. We have observed no excess γ -ray emission from Tri-II and upper limit has been derived on the γ -ray flux from Tri-II.

Using the DM halo modelling, we have further estimated the upper limits of photon flux and $\langle \sigma v \rangle$ by considering that the DM entirely consists of neutralinos. Our results show that in Tri-II, for $\sigma_v = 4.2 \text{ km sec}^{-1}$, 100% $b\bar{b}$ channel constrains mSUGRA and MSSM models with low thermal relic densities and Kaluza-Klein DM in UED and AMSB models with masses $\lesssim 230 \text{ GeV}$ and $\lesssim 375 \text{ GeV}$ respectively. It is important to note for the velocity dispersion with 90 % C.L. i.e. $\sigma_v = 3.4 \text{ km sec}^{-1}$ also constrains the MSSM model with low thermal relic densities and AMSB model with masses $\lesssim 300 \text{ GeV}$. We also find that analysis of gamma-ray data from Tri-II puts stronger limits on the DM models than UMi which justifies our choice of Tri-II for testing the DM models.

Here it is important to note that the data from UMi has been analysed in Figs. 3(a,b) and 4 by using the same parameters as were used previously in Ref. [3]. However, since the Fermi tools along with the IRF packages have been updated, we are not likely to exactly reproduce the results obtained in Ref. [3]. However, we have ensured the correctness of our results (in Figs. 3(a,b) and 4) by separately analysing Fermi-data on UMi for almost seven years with the use of the upgraded IRF. From that analysis, we have found that the LAT sensitivity, as obtained by us, scales by the similar factor as is expected while using data from 11 months (Ref. [59]). This provides confidence on the reliability of the analysis procedure adopted in the figures mentioned above. Hence, we can conclude that Tri-II may be better candidate for indirect DM search at energies greater than $\sim 300 \text{ GeV}$. We would like to mention another point that the results are based on the standard NFW halo shape and we do not take into account the effects of boost factor related to substructures in Tri-II or the Sommerfeld effect in accord to the annihilation cross-section. Finally, we can say that more precise observations of Tri-II in future would ultimately vindicate the possibility of establishing Tri-II as a candidate for indirect DM search.

Acknowledgement

We would like to thank Dr. James Unwin, Visiting Research Assistant Professor, University of Illinois at Chicago, IL, USA, for providing useful feedback which helps us to improve the present manuscript. We are grateful to Drs. Stefan Profumo and Tesla Jeltema of the University of California, Santa Cruz, USA for much needed help, advice and

guidance in the Fermi-LAT Data analysis.

-
- [1] E. Komatsu *et al.*, *Astrophys. J. Suppl.* **192**, 18 (2011).
- [2] P. A. R. Ade *et al.* [Planck Collaboration], *Astron. and Astrophys.* **594**, A13 (2016).
- [3] A. A. Abdo *et al.*, *Astrophys. J.* **712**, 147 (2010).
- [4] G. Steigman and M. S. Turner, *Nucl. Phys. B.* **253**, 375 (1985); G. Bertone, D. Hooper and J. Silk, *Phys. Rept.* **405**, 279 (2005).
- [5] G. Jungman, M. Kamionkowski and K. Griest, *Phys. Rep.* **267**, 195 (1996).
- [6] <http://fermi.gsfc.nasa.gov>.
- [7] J. Diemand, B. Moore and J. Stadel, *Nature (London)* **433**, 389 (2005).
- [8] M. Kuhlen *et al.*, *J. Phys. Conf. Ser.* **125**, 012008 (2008).
- [9] V. Springel *et al.*, *Nature (London)* **435**, 629 (2005).
- [10] M. L. Mateo, *Astron. and Astrophys.* **36**, 435 (1998); J. S. Gallagher *et al.*, *Astrophys. J.* **588**, 326 (2003); J. Grcevich and M. E. Putman, *Astrophys. J.* **696**, 385 (2009).
- [11] D. G. York *et al.*, *Astron. J.* **120**, 1579 (2000).
- [12] B. Willman *et al.*, *Astron. J.* **129**, 2692 (2005).
- [13] D. B. Zucker *et al.*, *Astrophys. J. Lett.* **650**, L41 (2006).
- [14] V. Belokurov *et al.*, *Astrophys. J.* **654**, 897 (2007).
- [15] M. J. Irwin *et al.*, *Astrophys. J. Lett.* **656**, L13 (2007).
- [16] S. M. Walsh, H. Jerjen and B. Willman, *Astrophys. J. Lett.* **662**, L83 (2007).
- [17] L. E. Strigari *et al.*, *Astrophys. J.* **678**, 614 (2008).
- [18] N. Kaiser *et al.*, Conference on Survey and Other Telescope Technologies and Discoveries, Waikoloa, Hawaii, August 27-28, (2002), *Proc. SPIE. Int. Soc. OPT. Eng.* **4836**, 154 (2002).
- [19] T. Abbott *et al.* [Dark Energy Survey], arXiv: 0510346v1 (2005).
- [20] B. P. M. Laevens *et al.*, *Astrophys. J. Lett.* **802**, L18 (2015).
- [21] K. Bechtol *et al.* [Dark Energy Survey], *Astrophys. J.* **807**, 50 (2015).
- [22] D. Kim and H. Jerjen, *Astrophys. J. Lett.* **808**, L39 (2015).
- [23] A. Drlica-Wagner *et al.* [Dark Energy Survey], *Astrophys. J.* **813**, 109 (2015).
- [24] A. Genina and M. Fairbairn, *Mon. Not. R. Astron. Soc.* **463**, 3630 (2016).
- [25] K. Hayashi *et al.*, *Mon. Not. R. Astron. Soc.* **461**, 2914 (2016).
- [26] N. F. Martin *et al.*, *Astrophys. J.* **818**, 40 (2016).
- [27] E. N. Kirby *et al.*, *Astrophys. J. Lett.* **814**, L7 (2015).
- [28] E. N. Kirby *et al.*, 2017 *Astrophys. J.* **838**, 83 (2017).
- [29] S. R. Majewski *et al.*, *Astrophys. J.* **615**, 738 (2004).
- [30] N. F. Martin *et al.*, *Astrophys. J.* **787**, 19 (2014).
- [31] A. J. Deason *et al.*, *Mon. Not. R. Astron. Soc.* **444**, 3975 (2014).
- [32] W. B. Atwood *et al.*, *Astrophys. J.* **697**, 1071 (2009).
- [33] <http://fermi.gsfc.nasa.gov/ssc/data/analysis/software>.
- [34] W. Cash, *Astrophys. J.* **228**, 939 (1979).
- [35] J. R. Mattox, *et al.*, *Astrophys. J.* **461**, 396 (1996).
- [36] https://fermi.gsfc.nasa.gov/ssc/data/analysis/documentation/Cicerone/Cicerone_LAT_IRFs/IRF_overview.html.
- [37] R. Essig, N. Sehgal, L.E. Strigari, *Phys. Rev. D*, **80**, 023506 (2009).
- [38] W. Rolke, A. Lopez, J. Conrad, *Nucl. Instrum. Methods A*, **551**, 493 (2005).
- [39] R. Barbieri, S. Ferrara and C. A. Savay, *Phys. Lett. B* **119**, 343 (1982).
- [40] E. A. Baltz *et al.*, *J. Cosmol. Astropart. Phys.* **07**, 13 (2008).
- [41] N. Arkani-Hamed *et al.*, *Phys. Rev. D* **79**, 015014 (2009).
- [42] J. L. Feng, M. Kaplinghat, and H. B. Yu, *Phys. Rev. D* **82**, 083525 (2010).
- [43] J. F. Navarro, C. S. Frenk, S. D. M. White, *Astrophys. J.* **490**, 493 (1997).
- [44] N. W. Evans, J. L. Sanders, A. Geringer-Sameth, *Phys. Rev. D*, **93**, 103512 (2016).
- [45] A. Charbonnier *et al.*, *Mon. Not. R. Astron. Soc.* **418**, 1526 (2011).
- [46] G. D. Martinez *et al.*, *J. Cosmol. Astropart. Phys.* **06**, 014 (2009).
- [47] T. E. Jeltema and S. Profuma, *J. Cosmol. Astropart. Phys.* **11**, 003 (2008).
- [48] A. H. Chamseddine, R. Arnowitt, P. Nath, *Phys. Rev. Lett.* **49**, 970 (1982).
- [49] D. J. H. Chung *et al.*, *Phys. Rep.* **407**, 1 (2005).
- [50] G. F. Giudice, R. Rattazi, M. A. Luty and H. Murayama, *J. High Energy Phys.* **12**, 027 (1998); L. Randall and R. Sundrum, *Nucl. Phys. B* **557**, 79 (1999).
- [51] H. C. Cheng, J. L. Feng, K. T. Matchev, *Phys. Rev. Lett.* **89**, 211301 (2002).
- [52] G. Servant and T. M. P. Tait, *Nucl. Phys. B* **650**, 391 (2003).
- [53] D. Hooper and S. Profumo, *Phys. Rep.* **453**, 29 (2007).
- [54] T. Moroi and I. Randall, *Nucl. Phys. B* **570**, 455 (2000).

- [55] M. Fujii and K. Hamaguchi, Phys. Rev. D **66**, 083501 (2002); M. Fujii and M. Ibe, Phys. Rev. D **69**, 035006 (2004).
- [56] P. Salati, Phys. Lett. B **571**, 121 (2003).
- [57] S. Profumo and P. Ullio, J. Cosmol. Astropart. Phys. **11**, 006 (2003).
- [58] G. Kane, R. Lu, and S. Watson, Phys. Lett. B **681**, 151 (2009).
- [59] E. Charles *et al.*, Phys. Rep. **636**, 1 (2016).